China Instrument and Control Society
Instrumentation
INSTRUMENTATION, Vol. 12, No. 2, June 2025
https://doi.org/10.15878/j.instr.202500259

Article

A Total Variational Image Denoising Model Coupled with a New Non-local Edge Extractor and a Level Set Curvature Gradient

Zhou Han[1], Xianchun Zhou[1*], Binxin Tang[2], Siqi Lu[2]

[1] School of Artificial Intelligence, Nanjing University of Information Science and Technology, Nanjing 210044, China

[2] School of Electronic and Information Engineering, Nanjing University of Information Science and Technology, Nanjing 210044, China

[*] Corresponding author email: 001398@nuist.edu.cn

Abstract: To solve the problem of false edges in a flat region of ℓ_1 norm total variational TV model, an edge extractor based on non-local idea is proposed in this paper. The new edge extractor can effectively suppress the influence of noise and extract the edge information of the image. The new edge extractor is used as the adaptive function and the weighting function of the ℓ_p norm variational model to control the noise reduction ability of the model, and a new model 1 is obtained. Considering that the new model 1 only uses the gradient mode as the image feature operator, which is insufficient to express the image texture information, a new level set curvature gradient variational model 2 combined with the edge extractor is proposed. The new model 2 uses the idea of minimum curvature of the level set of clear images to obtain noise reduction images. By coupling new model 1 and new model 2 to smooth the noise and protect more textures, a new Non-local level set denoising model (NLSDM) for image noise reduction is obtained. The experimental results show that compared with the noise reduction model, the new model has significantly improved the peak signal-to-noise ratio and structural similarity, and the effect of noise reduction and edge preservation is better.

Keywords: TV model; the ℓ_p norm; nonlocal; *p*function; level set curvature; term of regularization

Citation: Zhou Han, Xianchun Zhou, Binxin Tang, Siqi Lu."A Total Variational Image Denoising Model Coupled with a New Non-local Edge Extractor and a Level Set Curvature Gradient." Instrumentation 12, no.2 (June 2025). https://doi.org/10.15878/j.instr.202500259

1 Introduction

Image denoising serves as the foundation of image processing. Analyzing a clear image is of significant importance for improving the accuracy of image information recognition. However, noise is inevitably introduced during the processes of image acquisition, transmission, and processing, making image denoising the primary task in image processing. Currently, image-denoising methods can be broadly categorized into two main types. The first type consists of deep learning-based image denoising methods[1-3], which leverage neural network architectures for denoising. While these methods offer superior denoising performance, they have high hardware requirements and require longer processing times. The second type consists of traditional image denoising methods, which are further divided into transform domain and spatial domain approaches. In the transform domain, noise is treated as high-frequency information. Various transformations, such as wavelet transform[4,5], are employed to convert the image from the spatial domain to the transform domain. Noise coefficients are then eliminated by applying soft or hard thresholding. However, high-frequency coefficients contain not only noise but also signal information, so improper threshold selection may result in edge blurring or distortion. In the spatial domain, denoising methods include filtering techniques[6], non-local means denoising[7,8], and partial differential equation (PDE) - based methods[9-11]. Among these, PDE-based methods are supported by robust mathematical theories and offer

both denoising and edge-preserving capabilities, making them a crucial approach for denoising. The denoising method proposed in this paper belongs to the variational partial differential equation (VPDE) approach within PDE-based methods. The VPDE method performs a holistic analysis of the image, constructs an associated energy function, and transforms it into a variational problem for solution.

Among the variational partial differential methods, the TV model based on the ℓ_1 -norm[12]is the most representative. This paper builds upon the TV model to address issues of false edges and texture blurring in variational models. To overcome the limitations of the TV model, many scholars have proposed their improved models. Zhang Hongying et al. [13]proposed a new*p*-function based on the ℓ_p-norm variational model, which preserves more texture detail. However, the denoising performance of the model needs improvement. Wang Meiling et al. [14] proposed a total variation coupling model, which incorporates a trend fidelity term and combines wavelet transform to suppress the "staircase effect." However, the model still tends to blur edge and texture details. Huang Huan et al.[15] proposed a forward-backward diffusion variational model that enhances edge textures to some extent and preserves certain texture details. However, the denoising effect of the model requires further improvement. Zhou Xianchun et al. [16] proposed a curvature variational fidelity term based on wavelet transform. After enhancing the image using wavelet transform, the curvature of the level set of the enhanced image was used to construct a driving function and form a new fidelity term, which preserves more texture information. However, the model still exhibits a pronounced "staircase effect." Wang Na et al.[17]proposed a medical image denoising model based on a variable-order variational model. By introducing an edge indicator to control the variational order, the model suppresses speckle noise and stripe artifacts while blurring texture details in the image. Liu Pei et al. [18] proposed an enhanced high-order non-convex total variation image denoising model to address the "staircase effect" in images. This model preserves texture information but weakens the denoising capability. Huang Xiaoli et al.[19] proposed a model combining non-convex second-order total variation with overlapping group sparsity regularization. While it preserves more texture information, the denoising capability of the model requires improvement. Tang Binxin et al. [20]proposed a high-order total variation algorithm based on l_0-overlapping group sparsity, which effectively suppresses the staircase effect in smooth regions and preserves edge detail information. Zhou Xianchun et al. [21]proposed a texture-prior-based extended residual attention similarity denoising network, which greatly improves image visual quality and enhances practical applicability.

To preserve more texture details in images and address the issue of false edges in flat regions caused by the total variation model, this paper proposes the NLSDM denoising model, which couples a new non-local edge extractor with a level-set curvature gradient regularization term. First, based on the ℓ_p-norm variational model, a new non-local edge extractor is introduced. The non-local edge extractor serves as both the*p*-function and the weighting function for the ℓ_p-norm variational model, enabling control over the model's denoising capability. Secondly, considering that denoising models often rely solely on gradient magnitude as the feature detection operator, which inadequately represents detailed information, this paper proposes a level-set curvature gradient variational model combined with the non-local edge extractor. This model represents texture information jointly with the gradient. Finally, the NLSDM denoising model is formed by coupling the new non-local edge extractor with the level-set curvature gradient regularization term.

2 Related Work

2.1 TV Model Based on ℓ_1-Norm

Let *u*represent the denoised image, then the image denoising model based on the ℓ_1-norm is

$$\min_u E_2(u) = \iint_\Omega |\nabla u| dxdy + \frac{\lambda}{2}\iint_\Omega |u-v|^2 dxdy \quad (1)$$

Using the gradient descent method to solve Equation (1), the corresponding partial differential equation for the Euler-Lagrange equation is

$$\frac{\partial u}{\partial t} = \nabla\bullet\left(\frac{\nabla u}{|\nabla u|}\right) - \lambda(u-v) \quad (2)$$

Here, ∇represents the gradient operator, ∇•denotes the divergence operator, $\lambda$is the fidelity term coefficient, which controls the balance between the regularization term and the fidelity term, and *v*is the original image. In Equation (2), the TV model uses $1/|\nabla u|$ as the diffusion coefficient. Depending on the gradient values in flat regions and at the edges of the image, the diffusion rate varies, achieving noise reduction while preserving edges.

However, the TV model has the following shortcomings:

1) In Equation (1), the TV model uses only the gradient as the feature detection operator, which lacks sufficient expression of texture details and leads to the loss of such details.

2) In Equation (2), since the TV model performs diffusion along the edges, it generates false edges in flat regions, resulting in the "staircase effect."

2.2 TV Model Based on ℓ_p-Norm(ZTV)

Scholar Zhang Hongying proposed an image-denoising model based on the $\ell_p$norm as follows:

$$\min_u E_2(u) = \frac{1}{p}\iint_\Omega |\nabla u|^p dxdy + \frac{\lambda}{2}\iint_\Omega |u-v|^2 dxdy \quad (3)$$

Here, $p(x,y)=1+1/\left(1+\left|\nabla G_\sigma * v(x,y)\right|^2\right)$, $G_\sigma$is a Gaussian filter with a standard deviation ofσ.

Using the gradient descent method to solve equation (3), the corresponding partial differential equation for its Euler-Lagrange equation is: Using the gradient descent method to solve equation (3), the corresponding partial differential equation for its Euler-Lagrange equation is:

$$\frac{\partial u}{\partial t}=\nabla\bullet\left(\frac{\nabla u}{|\nabla u|^{2-p}}\right)-\lambda(u-v) \tag{4}$$

In formula (4), the p function performs diffusion in different forms in the flat regions and edge regions according to the characteristics of the image. In the flat regions, the p function approaches 2, and the model conducts isotropic diffusion, which avoids the problem of false edges existing in the flat regions of the TV model. At the edges, the p function approaches 1, and the model is transformed into the TV model to conduct anisotropic diffusion, preserving the edge information of the image. However, the ZTV model uses the gradient as the texture detection operator of the p function, which is insufficient in expressing the detailed texture information and will lead to the loss of the texture information of the image.

3 A total Variation Denoising Model Combining the ℓ_p-norm and Level Set Curvature Gradient Regularization

3.1 A Novelℓ_p-Norm Variational Denoising Model Based on a New Non-Local Edge Detector (New Model 1)

To address the issue of false edges in flat regions caused by the TV model, this study introduces improvements based on the ℓ_p-norm total variation (TV) model. Considering that the p-function typically uses gradient magnitude operators as image feature detectors, which lack sufficient detail expression, a new edge extractor based on non-local principles is proposed. The new non-local edge extractor is employed as both the p-function and the weighting function in the ℓ_p-norm total variation model.

To better extract image edges, a new edge extractor based on non-local principles is proposed, inspired by the non-local means denoising method. In the non-local means framework, the more similar the blocks, the higher their similarity. For noisy images, flat regions contain more noise, leading to lower similarity between blocks, while edges are more prominent, resulting in higher similarity. This study improves the exponential function parameters of the similarity measure by introducing adaptive parameters to better extract edge information.

First, apply Gaussian filtering to the noisy image, using a 3×3 neighborhood around each pixel. Then, using the surrounding neighborhood pixels as the center, a 5×5 neighborhood is taken. This results in 8 image matrices of size 5×5, and the similarity between blocks is calculated similarly to the non-local means approach. Here, the parameters of the exponential function are improved by selecting the mean of the adaptive Euclidean distance matrix as a parameter, which better extracts edge information. The improved similarity calculation expression is shown in Equation (5):

$$w(i,j)=\exp\left(-\frac{\left\|\vartheta(N_i)-\vartheta(N_j)\right\|_2^2}{h^2}\right) \tag{5}$$

Here, $w$represents the similarity between blocks$\vartheta(N_i)$and$\vartheta(N_j)$; $h$is the improved adaptive parameter, which is the mean of the Euclidean distance matrix$\left\|\vartheta(N_i)-\vartheta(N_j)\right\|_2^2$.

The similarity is obtained using formula (5). By taking a 3×3 neighborhood around the pixel, we obtain 8 similarity results between the neighborhood matrices and the center matrix. The average of these results gives the non-local similarity for the center pixel. This result is greater than 0 and less than 1.

To demonstrate the effectiveness of the new non-local edge extractor, we first use the original "cameraman" image as an example to compare the edge extraction results of common edge extractors: gradient magnitude operator, differential curvature operator, Laplacian operator, and the new non-local edge extractor. Since the ranges of the extractors differ, each extractor needs to be normalized and then multiplied by 255 for comparison. The result is shown in Figure 1.

From Figure 1, it can be observed that when edge extraction is performed on the original "cameraman" image, the new non-local edge extractor produces more distinct edges, making it more effective than the others.

Next, Gaussian white noise with a noise level of $\sigma=25$ is added to the "cameraman" image, and the edge extraction results are compared. The result is shown in Figure 2.

From Figure 2, it can be seen that when edge extraction is performed on the noisy "cameraman" image, the other three operators are more susceptible to noise and extract the noise along with the edges. However, in the result of the new non-local edge extractor, there is little noise, and the edge extraction is of superior quality. Based on the extraction results in Figure 1 and Figure 2, it can be concluded that the new edge extractor produces better results.

The new non-local edge extractor is used as the$p$function and weighting function in theℓ_p-norm total variation model, as shown in equation (6):

$$\frac{\partial u}{\partial t}=\nabla\bullet\left(\frac{\nabla u}{|\nabla u|^{2-p}}\bullet\left(\frac{1}{1+NL}\right)\right)-\lambda(u-v) \tag{6}$$

Here,$p=2-NL^{0.03}$.

In equation (6), $NL$is the new edge extractor for the image, used to extract the image's edges, with values in

(a) cameraman

(b) gradient mode

(c) differential curvature

(d) laplace

(e)new non-local edge extractor

Fig.1 Edge extraction of the cameraman image

(a) noisy cameraman

(b) gradient mode

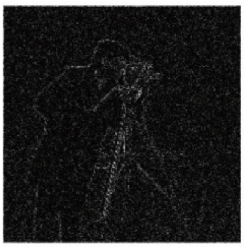

(c) differential curvature

(d) laplace

(e) new non-local edge extractor

Fig.2 Edge extraction of the noisy cameraman image

the range of [0, 1]. In flat regions, $NL \to 0$; at edges, $NL \to 1$. Therefore, by using $\frac{1}{1+NL}$as a weighting function and multiplying it with the diffusion term, the smoothing rate at the edges can be reduced, thus preserving the edges of the image. For the *p*function, in flat regions, $p \to 2$; in edge regions, $p \to 1$, achieving the goal of denoising while preserving edges.

3.2 A New Total Variation Denoising Model Combining Non-Local Edge Extractor and Level Set Curvature Gradient(New Model 2)

New Model 1 uses the gradient magnitude of the image as a regularization term. Considering the limitations of gradient magnitude in expressing image detail information, this paper proposes using the gradient of the image's level set curvature as another regularization term. For a noise-free image, its level set curvature is smooth. If noise is present in the image, the level set curvature will change. Therefore, the gradient of the image's level set curvature can be considered as a regularization term in the total variation model to smooth the noise. Additionally, a non-local edge extractor is used as a weighting function to preserve more image texture information.

The expression for the image's level set curvature is:

$$k = -div\left(\frac{\nabla u}{|\nabla u|}\right) = -\frac{u_{xx}u_y^2 - 2u_x u_y u_{xy} + u_{yy}u_x^2}{|\nabla u|^3} \tag{7}$$

Here, *div* is the divergence operator.

The expression for the gradient of the image's level set curvature as the regularization term in the total variation model is:

$$\min_u E_2(u) = \iint_\Omega |\nabla k| \bullet \left(\frac{1}{1+NL}\right) dxdy + \frac{\lambda}{2}\iint_\Omega |u-v|^2 dxdy \tag{8}$$

The corresponding partial differential equation for its Euler-Lagrange equation is:

$$\frac{\partial u}{\partial t} = \nabla \bullet \left(\frac{\nabla k}{|\nabla k|} \bullet \left(\frac{1}{1+NL}\right)\right) - \lambda(u-v) \tag{9}$$

The expression of the denoising model based on the image level set curvature gradient regularization term is given by formula (9).

3.3 Coupled denoising of New Model 1 and New Model 2 (NLSDM model)

By coupling New Model 1 and New Model 2, a new NLSDM image denoising model is obtained to preserve more image texture information. The expression of the new NLSDM model is as follows:

$$\begin{aligned}\frac{\partial u}{\partial t} &= a \bullet \left(\nabla \bullet \left(\frac{\nabla u}{|\nabla u|^{2-p}} \bullet \frac{1}{1+NL}\right)\right) \\ &+ (1-a) \bullet \left(\nabla \bullet \left(\frac{\nabla k}{|\nabla k|} \bullet \frac{1}{1+NL}\right)\right) - \lambda(u-v)\end{aligned} \tag{10}$$

Here, a is the coupling constant, with a range of 0 to 1. The value of a will be discussed later.

The new NLSDM model uses gradient magnitude and level set curvature as image texture detection operators, which helps preserve more texture information.

$$Tempx = \left(u_x^-.\hat{}2 + \left(\frac{\left(sign\left(u_y^-\right) + sign\left(u_y^+\right)\right).*\left(\min\left(abs\left(u_y^-\right), abs\left(u_y^+\right)\right)\right)}{2}\right)^2\right)^{\frac{1}{2}} \tag{11}$$

$$Tempy = \left(u_y^-.\hat{}2 + \left(\frac{\left(sign\left(u_x^-\right) + sign\left(u_x^+\right)\right).*\left(\min\left(abs\left(u_x^-\right), abs\left(u_x^+\right)\right)\right)}{2}\right)^2\right)^{\frac{1}{2}} \tag{12}$$

$$Divx = \frac{u_x^-}{Tempx} \tag{13}$$

$$Divy = \frac{u_y^-}{Tempy} \tag{14}$$

$$\frac{\partial u}{\partial t} = Divx_x^+ + Divy_y^+ \tag{15}$$

Here, u_x^- is the backward difference of the image u with respect to x, u_x^+ is the forward difference of the image u with respect to x. Similarly, u_y^- is the backward difference of the image u with respect to y, and u_y^+ is the forward difference of the image u with respect to y.

Then, based on the TV model, the discrete form of the new model 1 is obtained by using equation (5) to calculate the new non-local edge extractor and substituting it into equation (6). The discrete form of model 1 is:

$$Divx = \frac{u_x^-}{Tempx^{2-p}}.*\frac{1}{1+NL} \tag{16}$$

$$Divy = \frac{u_y^-}{Tempy^{2-p}}.*\frac{1}{1+NL} \tag{17}$$

$$\frac{\partial u}{\partial t} = Divx_x^+ + Divy_y^+ \tag{18}$$

The discrete form of the new model 1 is obtained from equation (18).

Then, based on the TV model, the discrete form of the new model 2 is derived.

First, discretize u_x, u_y, u_{xy}, u_{xx}, and u_{yy}. The expressions are:

$$u_x = \frac{u(x+1,y) - u(x-1,y)}{2} \tag{19}$$

$$u_y = \frac{u(x,y+1) - u(x,y-1)}{2} \tag{20}$$

$$u_{xx} = u(x,y+1) - 2*u(x,y) - u(x-1,y) \tag{21}$$

$$u_{yy} = u(x,y+1) - 2*u(x,y) - u(x,y-1) \tag{22}$$

$$u_{xy} = \frac{u(x-1,y-1) + u(x+1,y+1)}{4} - \frac{u(x-1,y+1) + u(x+1,y-1)}{4} \tag{23}$$

3.4 New Model Algorithm

In this paper, the discrete form of the new model is implemented based on the TV model algorithm. The discrete algorithm of the TV model is as follows, let:

Then, Substitute equations (19) - (23) into equation (7) to obtain the image's level set curvature k.

Substitute the level set curvature k into equations (12)-(15) to obtain the discrete form of the new model 2.

The new NLSDM model couples model 1 and the level set curvature gradient regularization term using the coupling constant a, thus obtaining the discrete form of the new NLSDM model.

The fidelity term coefficient λ for the three models is an adaptive fidelity term. The expression for λ is:

$$\lambda = \frac{1}{\sigma^2 * \mathrm{M} * \mathrm{Z}} \sum_x \sum_y \left(div.*\left(u - u_0\right)\right) \tag{24}$$

Here, div is $Divx_x^+ + Divy_y^+$; (M, Z) represents the size of the image; σ^2 is the noise level intensity of the image, which is obtained by calculating the difference between the images filtered by two different Laplacian filters.

3.5 Discussion on the Value of the Coupling Constant *a*

This paper discusses the value of the coupling constant a in the new NLSDM model using the cameraman and peppers images. The cameraman image is smooth and can be used to test the model's denoising capability, while the pepper image has clear textures and can be used to evaluate the model's ability to preserve textures. Figure 3 shows the cameraman and peppers images:

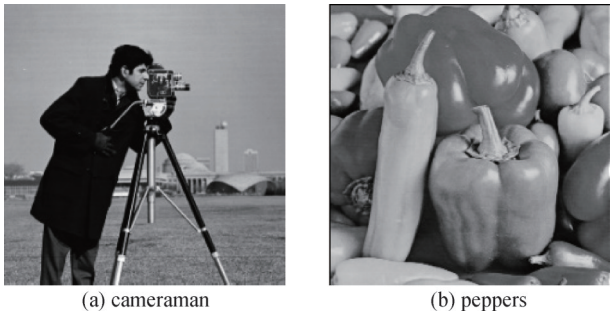

(a) cameraman (b) peppers

Fig.3 Cameraman image and pepper image

Gaussian white noise with standard deviations of $\sigma = 10$ and $\sigma = 40$ is added to the cameraman and pepper images

to create denoising experimental images. The Peak Signal-to-Noise Ratio (PSNR) values of the new NLSDM model are compared. The formula for Peak Signal-to-Noise Ratio (PSNR) is as follows:

$$PSNR = 10 \times \log_{10}\left(\frac{(2^n-1)^2}{MSE}\right) \tag{25}$$

In equation (25),

$$MSE = \frac{1}{mn}\sum_{i=0}^{m-1}\sum_{j=0}^{n-1}\| I(i,j) - K(i,j) \|^2 \tag{26}$$

m and n are the number of rows and columns of the image, $K(i,j)$ is the original image, and $I(i,j)$ is the denoised image. PSNR is based on the pixel-to-pixel error and indicates the quality of image denoising. The larger the value, the smaller the distortion.

Set the model parameters, with the time step $dt = 0.2$. For the same noisy image, adjust the coupling constant$a$in the new model 2 from 1 to 0, with an interval of 0.1. Table 1 shows the variation of PSNR values for noisy cameraman and peppers images with σ_n=10 and 40 as the coupling constant changes.

Table 1 the PSNR values of images with$\sigma_n = 10, 40$noise cameraman and peppers change with the coupling constant

a	0	0.1	0.2	0.3	0.4	0.5	0.6	0.7	0.8	0.9	1
Cameraman(10)	32.416	32.770	32.875	32.911	**32.919**	32.906	32.881	32.850	32.812	32.770	32.729
cameraman(40)	25.043	25.196	25.325	25.433	25.515	25.573	25.605	**25.609**	25.593	25.556	25.511
peppers(10)	33.610	33.853	33.964	34.025	**34.052**	34.046	34.017	33.974	33.909	33.836	33.758
peppers(40)	26.785	26.951	27.071	27.146	**27.190**	27.189	27.143	27.069	26.967	26.848	26.733

From Table 1, it can be seen that for the smooth cameraman image, the range of the coupling constant$a$varies from 0.4 to 0.7 as the noise intensity increases. For the texture-rich peppers image, the coupling constant$a$is set to 0.4 as the noise intensity increases. In this paper, the coupling constant$a$is chosen to be 0.5.

4 Result and Analysis

This paper uses six images, including a cameraman, as examples and conducts extensive simulation experiments using Matlab R2017b software. Among them, the cameraman and house images are relatively smooth and can be used to verify the denoising ability of the model; Ship and other images with prominent edges can be used to test the model's edge-preserving ability; City and other texture-rich images are used to detect the model's texture-preserving effect. During the experiment, Gaussian white noise with standard deviations of σ=10, 20, 30, and 40 is added to the original images as test images for denoising. Figure 4 shows the original images of the cameraman and the other five images:

To verify the effectiveness of the new NLSDM model, denoising experiments are conducted for comparison using the TV model, ZTV model, fourth-order LLT model, NLM algorithm, wavelet transform denoising, new model 1, and new model 2, demonstrating the denoising and edge-preserving capabilities of the new NLSDM model.

Compare the Peak Signal-to-Noise Ratio (PSNR) values and the Structural Similarity Index Measurement (SSIM) values of the above models.

The expression for Peak Signal-to-Noise Ratio (PSNR) is given in Equation (25), and the expression for Structural Similarity Index Measurement (SSIM) is as follows.

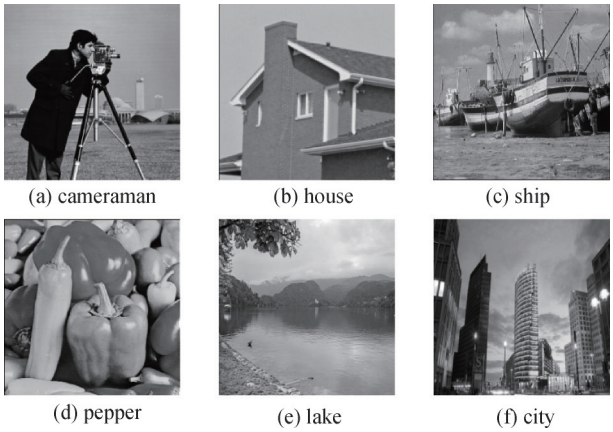

Fig.4 the six images including the cameraman
(a)cameraman(256×256); (b) house(256×256); (c) ship(512×512); (d)peppers(256×256); (e)lake(512×512); (f)city(512×512)

$$SSIM = \frac{(2\mu_K\mu_I + c_1)(\sigma_{KI} + c_2)}{(\mu_K^2 + \mu_I^2 + c_1)(\sigma_K^2 + \sigma_I^2 + c_2)} \tag{27}$$

In Equation (27),K is the original image, and$I$is the denoised image.μ_K is the mean of image K,μ_I is the mean of image I,σ_K^2 is the variance of K,σ_I^2 is the variance of I, and σ_{KI} is the covariance between K and I. $c_1 = (0.01L)^2$, $c_2 = (0.03L)^2$, $L = 255$。

SSIM is an index that measures the similarity between two images, with values ranging from (0,1). The more similar the two images are, the closer the SSIM value is to 1. Therefore, a higher SSIM value indicates better performance.

4.1 Objective Denoising Image Metrics Values

Based on the 6 original images in Figure 4, Gaussian white noise with standard deviations of σ=10, 20, 30, 40 is added, and denoising experiments are conducted using TV model, ZTV model, fourth-order LLT model, NLM

algorithm, wavelet transform (WT) denoising, new model 1, and new model 2 to demonstrate the denoising and edge-preserving ability of new model 2. Parameters are set to observe the Peak Signal-to-Noise Ratio (PSNR) and Structural Similarity Index (SSIM) of these models.

The time step $dt = 0.2$ is set to obtain the best Peak Signal-to-Noise Ratio (PSNR) and corresponding SSIM values for each model.

Table 2 shows the PSNR and SSIM values of the denoised images from the 8 models, with the best values in bold.

Table 2 comparison of experimental results with denoising models

PSNR(dB)/SSIM	$\sigma = 10$	$\sigma = 20$	$\sigma = 30$	$\sigma = 40$
cameraman	TV:32.833/0.891 ZTV:32.509/0.876 LLT:31.158/0.791 NLM:26.828/0.794 WT:26.198/0.753 model1:32.729/0.907 model2:32.416/0.875 NLSDM:**32.906/0.907**	TV:28.887/0.818 ZTV:28.751/0.809 LLT:26.682/0.680 NLM:26.502/0.775 WT:24.601/0.579 model1:29.205/**0.845** model2:28.674/0.793 NLSDM:**29.263**/0.840	TV:26.561/0.754 ZTV:26.495/0.747 LLT:24.126/0.547 NLM:25.742/0.728 WT:22.832/0.454 model1:26.987/**0.793** model2:26.493/0.736 NLSDM:**27.030**/0.786	TV:25.033/0.715 ZTV:24.987/0.707 LLT:22.380/0.437 NLM:24.909/0.645 WT:21.097/0.366 model1:25.511/**0.756** model2:25.043/0.691 NLSDM:**25.573**/0.748
house	TV:34.497/0.884 ZTV:34.289/0.876 LLT:31.843/0.799 NLM:29.899/0.819 WT:30.847/0.768 model1:34.414/0.879 model2:34.379/0.871 NLSDM:**34.749/0.885**	TV:31.425/0.839 ZTV:31.324/0.834 LLT:27.812/0.672 NLM:29.543/0.803 WT:27.0841/0.567 model1:31.625/0.846 model2:31.396/0.817 NLSDM:**32.010/0.848**	TV:29.520/0.810 ZTV:29.463/0.808 LLT:25.331/0.516 NLM:28.667/0.751 WT:24.089/0.423 model1:29.782/0.821 model2:29.462/0.773 NLSDM:**30.208/0.823**	TV:28.296/0.791 ZTV:28.251/0.787 LLT:23.357/0.407 NLM:27.344/0.654 WT:22.101/0.342 model1:28.575/0.804 model2:28.212/0.742 NLSDM:**28.996/0.806**
ship	TV:32.594/0.953 ZTV:32.401/0.951 LLT:31.998/0.902 NLM:27.196/0.845 WT:29.067/0.909 model1:32.661/0.958 model2:32.595/0.949 NLSDM:**32.881/0.958**	TV:29.285/0.897 ZTV:29.187/0.894 LLT:27.831/0.859 NLM:27.022/0.832 WT:26.243/0.765 model1:29.475/0.906 model2:29.423/0.888 NLSDM:**29.731/0.906**	TV:27.535/0.848 ZTV:27.483/0.847 LLT:25.496/0.779 NLM:26.683/0.809 WT:23.731/0.637 model1:27.732/0.859 model2:27.694/0.835 NLSDM:**27.991/0.859**	TV:26.227/0.804 ZTV:26.187/0.802 LLT:23.346/0.687 NLM:25.738/0.770 WT:21.723/0.538 model1:26.435/0.816 model2:26.379/0.787 NLSDM:**26.687/0.817**
peppers	TV:33.619/0.912 ZTV:33.405/0.904 LLT:31.549/0.833 NLM:28.179/0.842 WT:27.346/0.820 model1:33.758/0.919 model2:33.610/0.906 NLSDM:**34.046/0.921**	TV:29.896/0.856 ZTV:29.795/0.850 LLT:26.829/0.736 NLM:27.696/0.827 WT:25.332/0.652 model1:30.111/0.871 model2:30.137/0.853 NLSDM:**30.496/0.875**	TV:27.937/0.809 ZTV:27.874/0.806 LLT:24.669/0.603 NLM:27.075/0.787 WT:23.219/0.516 model1:28.167/0.830 model2:28.216/0.805 NLSDM:**28.587/0.836**	TV:26.473/0.771 ZTV:26.434/0.769 LLT:22.882/0.492 NLM:25.914/0.703 WT:21.451/0.421 model1:26.733/0.797 model2:26.785/0.768 NLSDM:**27.189/0.805**
lake	TV:33.302/0.938 ZTV:32.914/0.934 LLT:31.711/0.863 NLM:27.050/0.838 WT:28.815/0.862 model1:33.860/**0.948** model2:33.165/0.926 NLSDM:**33.978**/0.946	TV:29.629/0.875 ZTV:29.481/0.873 LLT:27.161/0.791 NLM:26.939/0.816 WT:26.110/0.660 model1:30.121/**0.893** model2:29.467/0.841 NLSDM:**30.166**/0.886	TV:27.724/0.826 ZTV:27.643/0.825 LLT:24.894/0.678 NLM:26.562/0.778 WT:23.749/0.511 model1:28.177/**0.849** model2:27.558/0.773 NLSDM:**28.188**/0.841	TV:26.421/0.788 ZTV:26.371/0.789 LLT:23.018/0.564 NLM:25.704/0.721 WT:21.765/0.408 model1:26.826/**0.814** model2:26.197/0.722 NLSDM:**26.827**/0.810
city	TV:32.749/0.957 ZTV:32.435/0.954 LLT:31.760/0.936 NLM:25.975/0.868 WT:27.375/0.893 model1:33.061/0.967 model2:32.704/0.947 NLSDM:**33.300/0.967**	TV:28.685/0.899 ZTV:28.572/0.899 LLT:27.097/0.870 NLM:25.821/0.848 WT:25.313/0.741 model1:29.006/**0.921** model2:28.698/0.880 NLSDM:**29.178**/0.915	TV:26.641/0.846 ZTV:26.580/0.846 LLT:24.853/0.775 NLM:25.511/0.818 WT:23.268/0.620 model1:26.940/**0.874** model2:26.733/0.824 NLSDM:**27.110**/0.866	TV:25.190/0.799 ZTV:25.155/0.797 LLT:22.984/0.680 NLM:24.743/0.768 WT:21.531/0.530 model1:25.499/**0.830** model2:25.342/0.777 NLSDM:**25.666**/0.824

By observing Table 2 and comparing the performance metrics of New Model 1 with the TV, ZTV, LLT models, NLM algorithm, and wavelet transform, it can be seen that the PSNR and SSIM values of New Model 1 are significantly higher than those of the other models, highlighting its superiority. However, there are a few exceptions. When Gaussian noise with a standard deviation of 10 is added to the cameraman and house images, the performance metrics of New Model 1 are slightly lower than those of the TV model. This suggests that New Model 1 may not be suitable for smooth images when the noise level is low. Overall, New Model 1 is well-suited for textured images or smooth images with higher noise levels, making it highly applicable in these cases.

When comparing the New NLSDM model with New Model 1, the PSNR value of New NLSDM is significantly higher, indicating that the coupling of the level-set curvature regularization term improves the denoising performance of the New NLSDM model. In terms of SSIM, the values for New NLSDM are slightly lower than those of New Model 1 in the cameraman, lake, and city images; however, the differences are negligible when compared to the increase in PSNR. Therefore, overall, the New NLSDM model performs better in denoising while preserving edges compared to New Model 1, and it also overcomes the limitation of New Model 1, which is less suitable for smooth images with low noise, making it more widely applicable.

4.2 Subjective Comparison of Denoised Images

Taking the cameraman and pepper images as examples, Gaussian white noise with a standard deviation of q=30 is added. The denoising results of eight models are compared in Figures 5 and 7, along with the corresponding local detail images in Figures 6 and 8. The cameraman image is relatively smooth, which allows for testing the denoising capability of the models; the pepper image, with richer textures, allows for testing the models' ability to preserve texture.

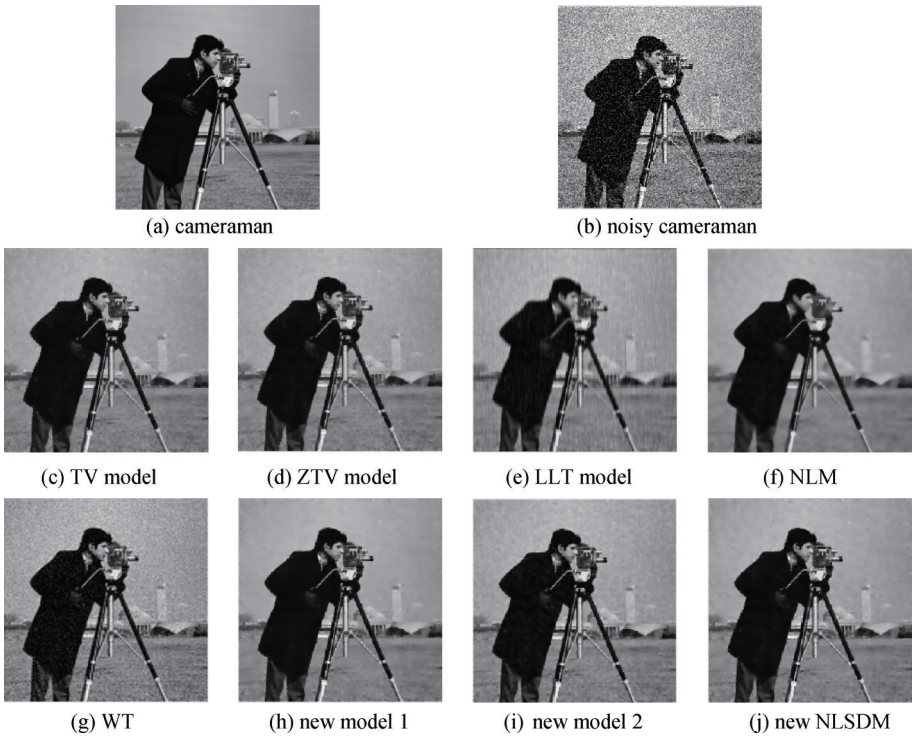

Fig.5 the denoising images of the Cameraman image

Observing the (j) images in Figures 5-8, it can be seen that the denoising results of the new NLSDM model exhibit overall good performance, with less noise, smoother images, and better denoising results. Compared to the denoising results of the TV, ZTV, and LLT models, as well as the NLM algorithm and wavelet transform, the new NLSDM model's result image has fewer noise points in flat areas, with sharper textures. Compared to the results of the new model 2, the new NLSDM model's result image shows clearer textures. While there is no obvious visible difference between the new NLSDM model's result and that of the new model 1, as shown in Table 2, the PSNR and SSIM values of the new NLSDM model have significantly improved. Therefore, the new NLSDM model demonstrates the best performance in denoising and edge preservation.

5 Conclusion

To address the issues of false edges and texture blurring in the ℓ_1-norm TV model, this paper introduces a total variation image denoising model coupled with a new

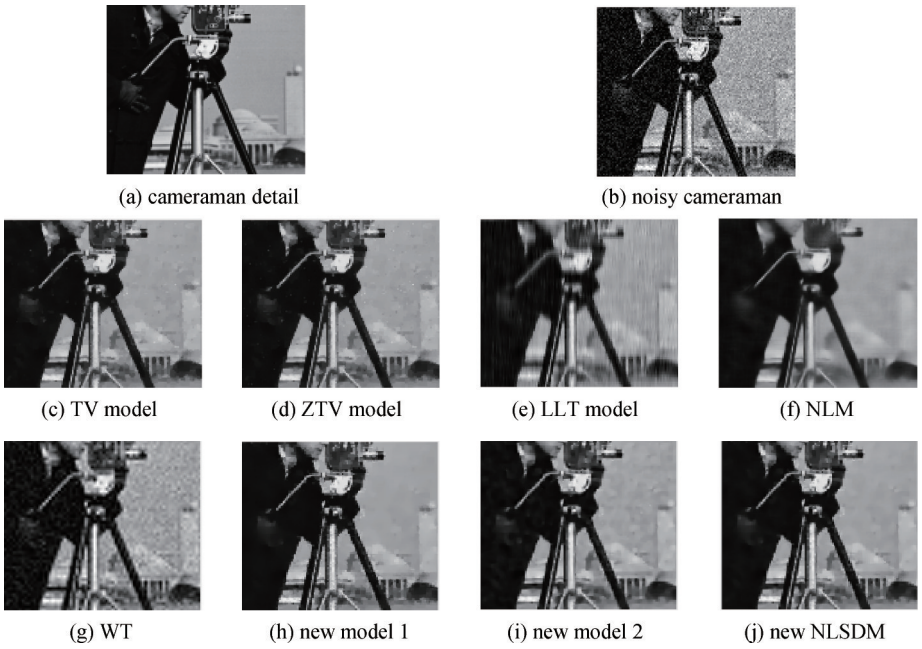

Fig.6 the denoising detail images of the Cameraman image

Fig.7 the denoising images of the peppers image

non-local edge extractor and the gradient of level-set curvature. Firstly, considering the false edge problem in flat regions of the TV model, a non-local-based edge extractor is proposed based on the ℓ_p-norm variational model. The new edge extractor effectively suppresses the influence of noise and extracts the edge information of the image. The new edge extractor is used as the adaptive$p$-function and weighting function for the ℓ_p-norm variational model to control the model's denoising ability, resulting in new model 1. Then, to address the

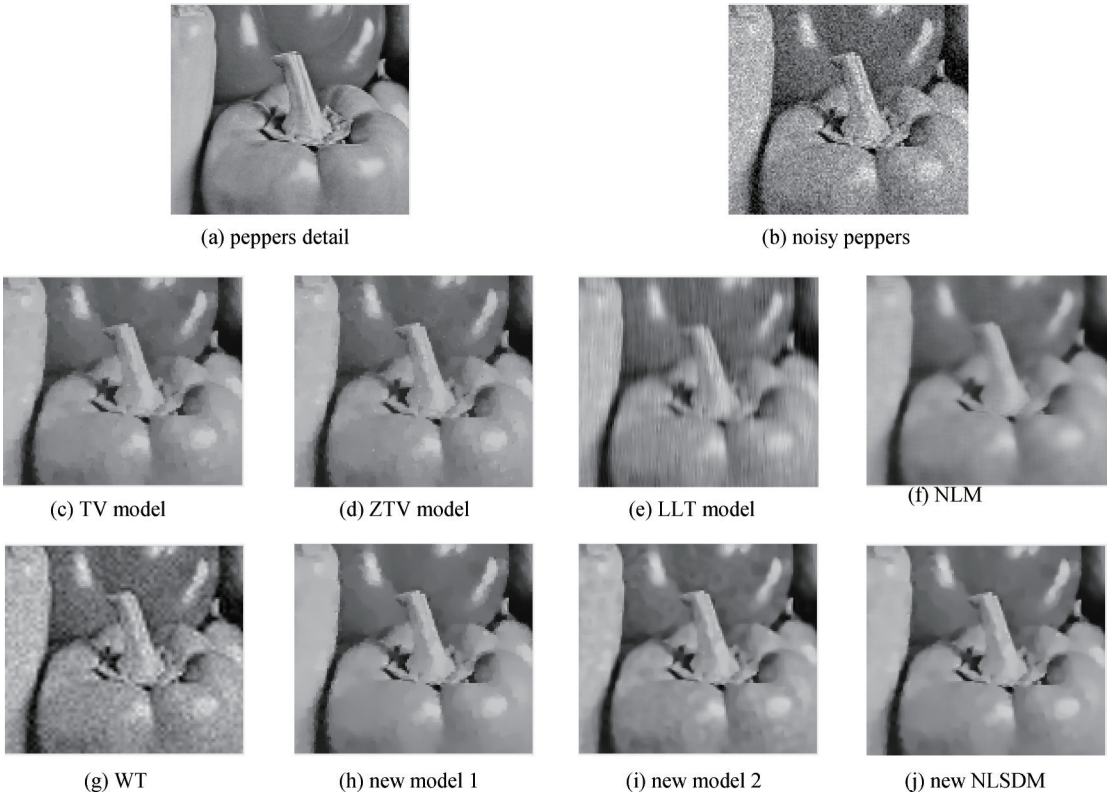

Fig.8 the denoising detail images of the peppers image

insufficient capability of capturing detailed information using only the gradient magnitude as the regularizer in ℓ_p-norm variational new model 1, a new level-set curvature gradient-based variational model 2 is proposed, which combines the edge extractor with the new regularizer. This new regularizer is coupled with the ℓ_p-norm regularizer to jointly protect the image's texture details. Finally, a discrete algorithm for the new model is introduced based on the TV model algorithm. Experimental results show that, compared to other denoising models, the new model achieves higher PSNR and SSIM values in objective denoising metrics; in terms of subjective denoising result images, the new model's output image has clear texture details and minimal noise. Therefore, the new model demonstrates the best performance in denoising and edge preservation.

Author Contribution:

Zhou Han: Took the lead in developing the research questions and overall study design. Conducted extensive raw data collection and led data analysis efforts. The core arguments and main findings of the paper are presented. Wrote most of the manuscript and coordinated the revision. Xianchun Zhou: Guide the research direction and provide valuable insights at every stage. Approve the final manuscript for submission. Binxin Tang: Additional experiments and validation were carried out. Helps create visual representations of data, such as charts. Participated in the discussion about the interpretation of the study and contributed to refining the conclusions. Siqi Lu: Oversaw the research progress and facilitated communication and collaboration among team members.

Foundation Information:

This research was funded by National Nature Science Foundation of China, grant number 61302188.

Data Availability:

The authors declare that the main data supporting the findings of this study are available within the paper and its Supplementary Information files.

Conflicts of Interest:

The authors declare no competing interests.

Dates:

Received 14 Decemeber 2024; Accepted 14 April 2025; Published online 30 June 2025

Appendix A: Formula Sheet

Numbering of Formula	Formula content	Explain
(1)	$\min_u E_2(u) = \iint_\Omega \lvert\nabla u\rvert dxdy + \frac{\lambda}{2}\iint_\Omega \lvert u-v\rvert^2 dxdy$	∇represents the gradient operator, ∇•denotes the divergence operator, $\lambda$is the fidelity term coefficient, which controls the balance between the regularization term and the fidelity term, and $v$is the original image.
(2)	$\frac{\partial u}{\partial t} = \nabla\bullet\left(\frac{\nabla u}{\lvert\nabla u\rvert}\right) - \lambda(u-v)$	
(3)	$\min_u E_2(u) = \frac{1}{p}\iint_\Omega \lvert\nabla u\rvert^p dxdy + \frac{\lambda}{2}\iint_\Omega \lvert u-v\rvert^2 dxdy$	$p(x,y) = 1 + 1/\left(1 + \lvert\nabla G_\sigma * v(x,y)\rvert^2\right)$, $G_\sigma$is a Gaussian filter with a standard deviation ofσ.
(4)	$\frac{\partial u}{\partial t} = \nabla\bullet\left(\frac{\nabla u}{\lvert\nabla u\rvert^{2-p}}\right) - \lambda(u-v)$	
(5)	$w(i,j) = \exp\left(-\frac{\left\lVert \vartheta(N_i) - \vartheta(N_j)\right\rVert_2^2}{h^2}\right)$	$w$represents the similarity between blocks$\vartheta(N_i)$and$\vartheta(N_j)$; $h$is the improved adaptive parameter, which is the mean of the Euclidean distance matrix$\left\lVert \vartheta(N_i) - \vartheta(N_j)\right\rVert_2^2$.
(6)	$\frac{\partial u}{\partial t} = \nabla\bullet\left(\frac{\nabla u}{\lvert\nabla u\rvert^{2-p}}\bullet\left(\frac{1}{1+NL}\right)\right) - \lambda(u-v)$	$p = 2 - NL^{0.03}$.
(7)	$k = -div\left(\frac{\nabla u}{\lvert\nabla u\rvert}\right) = -\frac{u_{xx}u_y^2 - 2u_x u_y u_{xy} + u_{yy}u_x^2}{\lvert\nabla u\rvert^3}$	*div* is the divergence operator.
(8)	$\min_u E_2(u) = \iint_\Omega \lvert\nabla k\rvert\bullet\left(\frac{1}{1+NL}\right)dxdy + \frac{\lambda}{2}\iint_\Omega \lvert u-v\rvert^2 dxdy$	
(9)	$\frac{\partial u}{\partial t} = \nabla\bullet\left(\frac{\nabla k}{\lvert\nabla k\rvert}\bullet\left(\frac{1}{1+NL}\right)\right) - \lambda(u-v)$	Denoising model based on the image level set curvature gradient regularization term.
(10)	$\frac{\partial u}{\partial t} = a\bullet\left(\nabla\bullet\left(\frac{\nabla u}{\lvert\nabla u\rvert^{2-p}}\bullet\frac{1}{1+NL}\right)\right) + (1-a)\bullet\left(\nabla\bullet\left(\frac{\nabla k}{\lvert\nabla k\rvert}\bullet\frac{1}{1+NL}\right)\right) - \lambda(u-v)$	$a$is the coupling constant, with a range of 0 to 1.
(11)	$Tempx = \left(u_x^-.\text{^}2 + \left(\frac{\left(sign\left(u_y^-\right) + sign\left(u_y^+\right)\right).*\left(\min\left(abs\left(u_y^-\right), abs\left(u_y^+\right)\right)\right)}{2}\right)^2\right)^{\frac{1}{2}}$	
(12)	$Tempy = \left(u_y^-.\text{^}2 + \left(\frac{\left(sign\left(u_x^-\right) + sign\left(u_x^+\right)\right).*\left(\min\left(abs\left(u_x^-\right), abs\left(u_x^+\right)\right)\right)}{2}\right)^2\right)^{\frac{1}{2}}$	u_x^- is the backward difference of the image$u$with respect to$x$, u_x^+ is the forward difference of the image u with respect to$x$. Similarly, u_y^- is the backward difference of the image u with respect to$y$, and u_y^+ is the forward difference of the image u with respect to$y$.
(13)	$Divx = \frac{u_x^-}{Tempx}$	
(14)	$Divy = \frac{u_y^-}{Tempy}$	
(15)	$\frac{\partial u}{\partial t} = Divx_x^+ + Divy_y^+$	

续表

Numbering of Formula	Formula content	Explain
(16)	$Divx=\frac{u_x^-}{Tempx^{2-p}}.*\frac{1}{1+NL}$	
(17)	$Divy=\frac{u_y^-}{Tempy^{2-p}}.*\frac{1}{1+NL}$	
(18)	$\frac{\partial u}{\partial t}=Divx_x^+ + Divy_y^+$	
(19)	$u_x=\frac{u(x+1,y)-u(x-1,y)}{2}$	
(20)	$u_y=\frac{u(x,y+1)-u(x,y-1)}{2}$	
(21)	$u_{xx}=u(x,y+1)-2*u(x,y)-u(x-1,y)$	
(22)	$u_{yy}=u(x,y+1)-2*u(x,y)-u(x,y-1)$	
(23)	$u_{xy}=\frac{u(x-1,y-1)+u(x+1,y+1)}{4}-\frac{u(x-1,y+1)+u(x+1,y-1)}{4}$	
(24)	$\lambda=\frac{1}{\sigma^2*\mathrm{M}*\mathrm{Z}}\sum_x\sum_y(div.*(u-u_0))$	div is $Divx_x^+ + Divy_y^+$;(M,Z)represents the size of the image;σ^2 is the noise level intensity of the image
(25)	$PSNR=10\times\log_{10}\left(\frac{(2^n-1)^2}{MSE}\right)$	PSNR is based on the pixel-to-pixel error
(26)	$MSE=\frac{1}{mn}\sum_{i=0}^{m-1}\sum_{j=0}^{n-1}\|I(i,j)-K(i,j)\|^2$	m and n are the number of rows and columns of the image,$K(i,j)$ is the original image, and $I(i,j)$ is the denoised image.
(27)	$SSIM=\frac{(2\mu_K\mu_I+c_1)(\sigma_{KI}+c_2)}{(\mu_K^2+\mu_I^2+c_1)(\sigma_K^2+\sigma_I^2+c_2)}$	$K$is the original image, and$I$is the denoised image. μ_K is the mean of image K, μ_I is the mean of image$I$,σ_K^2 is the variance of K,σ_I^2 is the variance of I, and σ_{KI} is the covariance between K and I.$c_1=(0.01L)^2$,$c_2=(0.03L)^2$,$L=255$。

References

[1] Zeng X H, Li Y C, Gao G, et al. Channel adaptive ultrasonic image denoising method based on residual codec[J]. *Journal of Electronics and Information Technology*, **2022**, 44(07): 2547-2558.

[2] Guan X Y, Hu W, Fu H. Remote sensing image denoising algorithm based on multi-receptive field feature fusion and enhancement[J].*Acta Photonica Sinica*,**2022**, 51(11): 365-377.

[3] Sagawa H, Fushimi Y, Nakajima S, et al. Deep Learning-based Noise Reduction for Fast Volume Diffusion Tensor Imaging: Assessing the Noise Reduction Effect and Reliability of Diffusion Metrics[J]. *Magnetic Resonance in Medical Sciences*, **2020**, 20(4): 450-456.

[4] Choi H, Jeong J. Despeckling Images using a Preprocessing Filter and Discrete Wavelet Transform-Based Noise Reduction Techniques[J]. *IEEE Sensors Journal*, **2018**, 18(8): 3131-3139.

[5] Xiao J, You S H. Research on Denoising method of engine surface defect image based on wavelet transform[J]. *Surface Technology* , **2018**, 47(12): 328-333.

[6] Zhang X F, Yan H. Image denoising and enhancement algorithm based on median filter and fractional filter[J]. *Journal of Northeastern University (Natural Science Edition)*, **2019**, 41(04): 482-487

[7] Xiao S, HU J, WANG Y F. Elliptic window and parameter adaptive non-local mean algorithm[J]. *Journal of Computer Aided Design and Graphics*, **2019**, 32(01): 79-89.

[8] Wang G, Yang L, Wei X, et al. An improved non-local means filter for color image denoising[J]. *Optik - International Journal for Light and Electron Optics*, **2018**, 173: 157-173.

[9] Hadri A, Afraites L, Laghrib A, et al. A novel image denoising approach based on a non-convex constrained PDE: application to ultrasound images[J]. *Signal Image and Video Processing*, **2021**, 15(5): 1057-1064.

[10] Barbu T. A Nonlinear Second-order Hyperbolic PDE-based Photon- limited Medical Microscopy Image Restoration Technique[J]. *Romanian Journal of Information Science and Technology*, **2020**, 23(S): 67-76.

[11] Zhou X C, WANG M L, SHI L F. High-fidelity anisotropic filter model for Threshold optimization[J]. *Journal of Computer-Aided Design and Graphics*, **2016**, 28(09): 1550-1559.

[12] Rudio L, Osher S, Fatemi E. Nonlinear total variation based noise removal algorithm[J]. *Physica D Nonlinear Phenomena*, **1992**, 60(1-4): 259-268.

[13] Zhang H Y, Peng Q Z. Total variational adaptive image denoising model[J]. *Opto-electronic Engineering*, **2006**(03): 50-53.

[14] Wang M L, Zhou X C, Zhou L F, et al. Total variational coupling image denoising model[J]. *Journal of Communications*, **2016**, 37(04): 182-191.

[15] Huang H, Nie Q W. Variational denoising based on forward and backward diffusion model [J]. *Journal of Yunnan University* (*Natural Science Edition*), **2016**, 38(03): 369-375.

[16] Zhou X C, Wu T, Shi L F, et al. A wavelet transform image denoising method based on curvature variational regularization[J]. *Acta Electronica Sinica*, **2018**, 46(03): 621-628.

[17] Wang N, Zhang Q, Liu Y, et al. Medical low-dose CT image denoising based on variable order variational model[J]. *Journal of Beijing University of Aeronautics and Astronautics*, **2019**, 45(09): 1757-1764.

[18] Liu P, Jia J, Chen L, et al. Image denoising algorithm based on enhanced high-order non-convex total variational model [J]. *Systems Engineering and Electronics*, **2019**, 42(03): 557-567.

[19] Huang X L, Chen C M, Liu G H. Noise reduction method of anti-nuclear radiation image with mixed second-order total variational[J]. *Journal of Chongqing University of Posts and Telecommunications (Natural Science Edition)*, **2022**, 34(04): 585-594.

[20] Tang B X, Zhou X C, Cui C C, et al. High Order Total Variational Denoising Algorithm Based on l0 Overlapping Combination Sparse[J]. *Instrumentation*,**2024**,11(03):30-40.

[21] Zhou X C, Shi Z T, Wang Z W, et al. Expanded residual attention similarity denoising network based on texture prior [J]. *Journal of Electronic Measurement and Instrumentation*, **2024**,38(05):75-89.